Ceramics International 49 (2023) 24611–24619

Contents lists available at ScienceDirect

Ceramics International

journal homepage: www.elsevier.com/locate/ceramint

Three sustainable polypropylene surface treatments for the compatibility optimization of PP fibers and cement matrix in fiber-reinforced concrete

Beatrice Malchiodi [a,b,*], Riccardo Pelaccia [c], Paolo Pozzi [a], Cristina Siligardi [a,b]

[a] Department of Engineering Enzo Ferrari, University of Modena and Reggio Emilia, Modena, Italy
[b] National Interuniversity Consortium of Materials Science and Technology INSTM, Florence, Italy
[c] Department of Sciences and Methods for Engineering, University of Modena and Reggio Emilia, Reggio Emilia, Italy

ARTICLE INFO

Handling Editor: Dr P. Vincenzini

Keywords:
Composite construction materials
Fiber reinforced concrete
Polypropylene fibers
Surface treatments
Functionalization
Hydrophilicity
Adhesion
Picosecond LASER
UV-LED
Corona discharge

ABSTRACT

Fiber-reinforced concrete (FRC) is a cementitious composite material that is gaining interest in the construction field to limit crack propagation and increase toughness. Polypropylene (PP) fibers are promising alternatives to steel fibers, primarily used in FRC, as they reduce weight and cost and are resistant to corrosion. However, the hydrophobic surface of PP inhibits a good adhesion with the surrounding cementitious matrix and so the exploitation of optimized mechanical performance. Though several chemical treatments have been studied, this work suggests more sustainable, cost-efficient, and fast surface treatments for the first time to increase the hydrophilicity of PP: UV-LED, picosecond UV-LASER, and corona discharge treatment. The treatments mainly provided a chemical functionalization without altering the surface morphology of PP, and their effectiveness in increasing PP hydrophilicity was confirmed by ATR-FTIR spectroscopy and optical contact angle measurements. The improved adhesion with the matrix was assessed by the pullout test of treated PP specimens from lime-based and cement-based matrices and by detecting the failure mode in the interphase zone through scanning electron microscopy.

Concrete is the most used construction material worldwide and, thanks to its unrivalled properties (i.e., cost-effectiveness, versatility, easy technology, etc.), its demand is expected to increase further to meet the growing demand for structures and infrastructures in new emergent Countries. On the other hand, the high demand for concrete is significantly responsible for CO_2 emissions, i.e., 8% of global CO_2 emissions [1]. Great efforts are spent to decarbonize the construction sector, including using secondary raw materials, more sustainable blend cement, and optimized concrete mix design and structural design [1]. Among these, the reduction of concrete demand per build-up area could be allowed by increasing concrete durability and mechanical performance. Hence, extending the service life of concrete structures and reducing the cross-section of concrete structural elements without affecting the overall strength of the structure, respectively. In recent decades Fiber Reinforced concrete (FRC), and more generally Fiber Reinforced Cementitious Composites (FRCC), have attracted interest due to their outstanding performance in improving the resistance to degradation and mechanical strength of the cementitious matrix. FRC and FRCC are composite materials mainly applied in the construction sector, which are made of a ceramic matrix (i.e., concrete, mortar) and a fiber reinforcement. As for steel-reinforced concrete, FRC can be defined as ceramic matrix composite (CMC). [2]. Apart from the mechanical properties, the fiber reinforcement can modulate the property of FRC and provide additional features such as low thermal conductivity, electrical conductivity, heat resistance, fire resistance, wear resistance, corrosion resistance, etc. [3,4]. Depending on the fiber type (i.e., steel, glass, carbon, synthetic) and content, the resulting FRC can display a reduction in cracks formation and propagation, an increase in stiffness and strength, or an increase in toughness. The first property is generally associated with microfibers, low fiber contents, and polymeric fibers. The second refers to fibers with a higher strength than the matrix, while the third relates to fibers with less stiffness than the matrix. In general terms, fibers act a crack-bridging effect allowing for the transfer of local stresses beyond cracks and their redistribution in still-resistant regions. By limiting the width of single cracks, the fibers distribute the stresses allowing for narrower and more scattered crack patterns throughout the matrix [5].

The crack-bridging effect relies on the capability of fibers to dissipate energy through friction while being pulled under direct or indirect tensile action. The phenomenon can be described assuming that the fiber

* Corresponding author. Department of Engineering Enzo Ferrari, University of Modena and Reggio Emilia, Modena, Italy.
E-mail address: beatrice.malchiodi@unimore.it (B. Malchiodi).

https://doi.org/10.1016/j.ceramint.2023.02.105
Received 7 October 2022; Received in revised form 31 January 2023; Accepted 13 February 2023
Available online 15 February 2023

is frictionally bonded to the matrix in which it is embedded and that the fiber debonding occurs through the activation of progressive interfacial frictional slip. The most common mechanical models used to describe the crack bridging effect state its dependence on interface shear stress, interface local slippage and fiber geometry. Also, they mainly correlate a higher interface shear stress to fiber surface abrasion, fragmentation of surface coatings and chemical bonding [6].

Compared to the most used steel fibers, polypropylene (PP) fibers provide FRC toughness, lightweight, anti-spalling properties (fire resistance), chemical resistance to alkaline environments [7], and shrinkage reduction. They are also cost-efficient, easily available, and do not corrode. Nevertheless, the a-polar nature of PP inhibits the proper wettability and adhesion of PP fibers with the cementitious matrix. Several methods have been studied to improve it, either by altering the surface polarity of the fiber or increasing its roughness. The results are promising, but the most studied and effective surface treatments mainly include chemical etching and coating deposition, while the characterization techniques primarily focus on mechanical properties. [8,9]. A more sustainable approach for functionalizing PP fibers would consist of surface treatments with no added chemicals; this would also be more feasible for industrial applications. For the first time, this work suggests alternative, fast, no added chemicals and cost-efficient treatments to increase the hydrophilicity and wettability of PP, thus enhancing its adhesion with the cementitious matrix and optimizing the mechanical properties of PP-FRC. For this purpose, three surface treatments with different highlights were considered: UV-LED, picosecond LASER, and corona discharge.

The UV-LED treatment is a photo-oxidation process, i.e., a photochemical reaction in the presence of oxygen, that increases the polarity and hydrophilicity of polyolefins. It provides high-energy radiation capable of splitting the -C-C and C–H covalent bonds, thus resulting in the formation of reactive radicals and a reduction in the molecular weight of the polymeric surface. The radicals react in the presence of oxygen and generate oxidized groups responsible for an increase in surface polarity. For each polymer, there is a characteristic wavelength range that leads faster to photo-oxidation; for PP the range is between 280 nm and 370 nm.

The corona discharge treatment is an industrial process used for polyolefins films (such as PP and PE) to increase wettability before printing or gluing. The treatment is successful in it by allowing the formation of carboxyl (-COOH), carbonyl (C═O), hydroxyl (-OH), and ester (–COO–) functional groups. It is performed using a generator, a transformer, and a set of electrodes (high-voltage electrode and ground electrode). A potential difference is generated between the electrodes, and high-frequency current discharges occur. The discharge of high-frequency electrons on the desired surface breaks the surface macromolecules and creates reactive radicals. These radicals then react with the oxygen in the air and generate oxidized functional groups on the treated polyolefin surface. The corona discharge treatment does not affect the strength and appearance of the treated surface. And it is a fast, cost-efficient, and effective treatment. Nevertheless, the process ionizes the air and the functionalization effect decades over time [10–12].

The LASER treatment ablates the specimen surface with a focused LASER beam of a specific wavelength. In the context of the ultrashort LASER, the combination of proper LASER parameters (power [W], repetition rate [KHz], scan speed [mm/s]) and the scanning strategy allow obtaining the surface texturing at the micro and nanoscales without altering the mechanical properties of the bulk material at the macroscales [13]. The main advantages of this technology are the absence of contact and consequently the contamination of the treated surface, the reduced treatment exposition, the easy automation that offers the opportunity to treat large areas, and the low environmental impact [13,14]. Notably, LASER texturing became an efficient and reliable technique to modify the wettability of different materials such as metals, ceramics, and polymers [14–16]. About the latter, some studies have investigated the effects of LASER texturing on PP wettability, taking advantage of the generation of topographical and chemical alterations [17,18].

In this context, the ultimate goal of this work is to characterize the PP surface after the three selected treatments thoroughly and to link the chemical and physical alterations to the mechanical performance of the composite material (i.e., PP-FRC). Dog-bone PP specimens instead of fibers were considered to avoid the influence of the fiber shape, thus easing the treatment and characterization of the PP surface. Contact angle, ATR-FTIR, and ESEM were involved in the surface characterization. Additionally, a 28-day pullout test was carried out for PP specimens embedded into mortars to highlight the effects of surface functionalization on the chemical and frictional adhesion of PP-FRC.

1. PP specimens

Polypropylene (PP) flat supports were considered instead of PP fibers to avoid the influence of fiber shape, thus simplifying the PP surface treatment and characterization. Therefore, dog-bone PP specimens (Fig. 1) were manufactured by injection molding using homopolymer PP granules by INEOS Olefins & Polymers Europe with a density of 0.91 g/cm^3. As displayed by the CAD drawing in Fig. 1, the PP specimens were 75 mm long, 9.9 mm wide and 2 mm thick. The manufacturing was performed using the injection molding machine Mega Tech H7/18–1 (Tecnicaduebi Srl) and considering the setting parameters from Table 1.

The PP specimens were then lapped with SiC papers (from P800 to P2500) and polished with colloidal diamond suspension (~3 μm size) to remove manufacturing defects and surface roughness. In the end, they were ultrasonically cleaned in acetone for 3 min and dried with compressed air.

Three surface treatments were considered to increase the compatibility of PP with cementitious matrices, namely UV-LED (2.1.1), picosecond LASER treatments (2.1.2), and corona discharge (2.1.3). These were expected to increase the polarity and hydrophilicity of PP through surface functionalization (oxidation and photo-oxidation) and so increase the wettability and adhesion with cementitious matrixes. All the treated PP specimens were kept in a vacuum desiccator until their characterization.

The wettability of the treated PP specimens was assessed through Optical Contact Angle (OCA) by Dataphysic and compared to that of the untreated one. The test was performed using a 3.5 μl drop of distilled water, and the contact angle image was acquired after 10 s using SCA20 software. Three measurements for each specimen were performed, and the average and standard deviation were assessed.

ATR-FTIR spectroscopy (ATR-FTIR VERTEX 70 by Bruker Optics, Ettlingen, Germany) was involved in detecting the oxidized groups characteristic of treated PP specimens compared to the untreated ones. Opus 6.5 by Bruker Optics GmbH allowed the analysis of the spectra, which were acquired after 32 scans, with a 4 cm^{-1} resolution, and in a 600 - 4000 cm^{-1} transmittance range.

Optical microscopy (CTR 4000 Leica, 100x) was involved to eventually detect morphological alteration brought by the treatments on the PP surface. Higher magnifications through optical or scanning electron microscopy were not considered because the main effects expected of the involved surface treatments were functionalizing and not morphological.

1.1. UV-LED treatment

The UV treatment was performed using a UV LED lamp by Photo Electronics with a peak wavelength of 395 nm and maximum irradiance of 12 W/cm^2. The UV lamp was fixed at 65 mm high to the specimens and set at the maximum irradiance value. A cold air source was installed at 20 cm from the specimens to reduce heat on the PP surface and limit the maximum surface temperature to 50 °C. In addition, the specimens were lifted from the support by plastic clamps to encourage air circulation on the specimen surface not exposed to radiation (Fig. 2a).

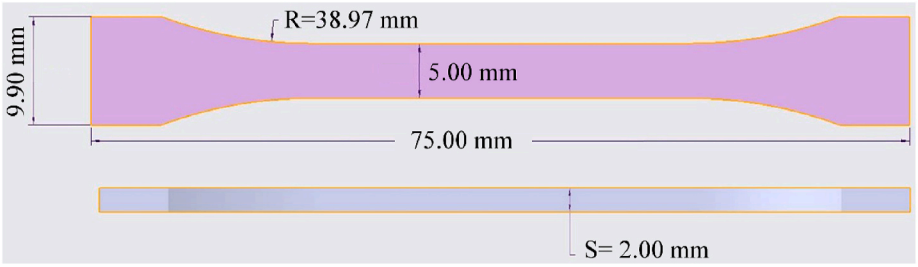

Fig. 1. Geometry of the PP specimen manufactured by injection molding.

Table 1
Manufacturing parameters for the injection molding process.

Temperature [°C]		Time [s]	
Hopper	200	Mold Retention	9
Screw	240	Maintenance	3
Cylinder	220		
Nozzle	220		

Different exposition times were considered for UV-LED treatment of PP, namely 6 h, 12 h, 24 h and 36 h. The setup of UV-LED treatment is shown in Fig. 2b.

1.2. LASER treatment

LASER treatments were performed using a picosecond amplifier EKSPLA Atlantic 5 LASER, which allows three beamlines (1064, 532, and 355 nm) with a pulse duration of about 10 ps. In this work, the 355 nm beamline was employed to guarantee the maximum energy absorption for polymeric materials [9]. Along the optical path of each beamline, a beam expander is inserted to obtain a beam diameter of 15 mm at the entrance of the galvanometric scanner. Raylase Superscan V galvanometric scanner coupled with a 104 mm F-theta lens allowed a focused beam with a $1/e2$ spot diameter of 10 μm and a working area of 46 × 46 mm on the specimen surface. However, since the LASER system is integrated with a 3-axis (X-Y-Z) movement system, it is possible to move the worktable to increase the working area during the LASER treatment.

The LASER treatment ablated the specimen surface following overlapped parallel scanlines perpendicular to the long side of the PP specimen. Keeping the movement system fixed, it was possible to treat three specimens simultaneously (Fig. 3b) in a few seconds or minutes, depending on the selected process parameters (Table 2). The scanner strategy was chosen to generate a uniform pulse distribution and so a uniform energy deposition on the specimen surface. Notably, the combination of scanner speed (500 mm/s), pulse repetition rate (100 kHz), and distance between two consecutive scanlines (5 μm) was selected to obtain an overlapping of 50% between two successive pulses on the

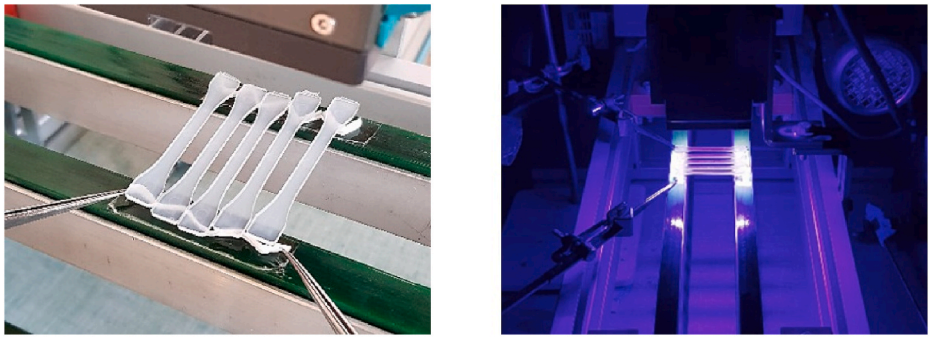

(a) (b)

Fig. 2. UV-LED treatment of PP specimens: a) positioning of dog-bone PP specimens, b) treatment setup.

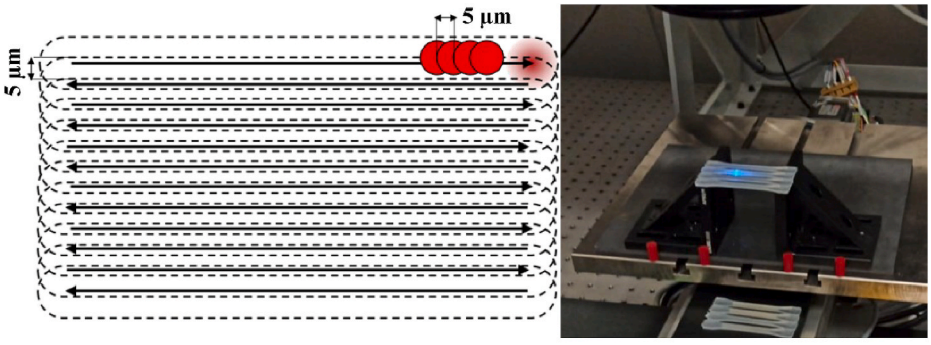

(a) (b)

Fig. 3. Picosecond LASER treatment: a) schematization of the scanner pulses distribution, b) treatment of dog-bone PP specimens.

Table 2
Process parameters of the six LASER treatment conditions.

Power [%]	Power [mW]	Pulse energy [μJ]	Macroscopic evidence [−]
5	1	0.01	No ablation
10	8	0.08	No ablation
15	18	0.18	Slight ablation
25	56	0.56	Ablation without burns
30	84	0.84	Ablation without burns
40	140	1.4	Significant ablation and burns

entire treated surface (Fig. 3a). The processing time to treat three specimens at once was 80 s with the selected kinematic configuration.

Six levels of LASER power were tested, starting from a low value (5%) that caused no visible signs of ablation on the surface to a threshold value (40%) that caused significant burns on the specimen (Fig. 4). Table 2 summarizes the process parameters for all six tested conditions. The last condition (40% of LASER power) was not considered for the functionalization of the PP surface to avoid possible random results due to burning.

1.3. Corona discharge treatment

The corona discharge treatment was carried out using the BD-20ACV corona discharge instrument from Electro technic products, equipped with a field-effect electrode (suitable for treating both flat and curved surfaces). The device consists of a Bakelite gun containing the generator, electronic-mechanical groups, and the field effect electrode at one end. The power supply unit is separate. In addition, an aluminum plate was used as the second electrode, on which the specimens were placed individually. The experimental setup for the corona discharge treatment is displayed in Fig. 5.

Based on literature evidence, the most effective discharge voltage was 35 kV [11]. Since the involved instrument could not directly set the discharge voltage value, a correlation with the spark length was found. Referring to the instrument datasheet, a discharge voltage of 35 kV was associated with a spark length of 18 mm. Several trial setups were tested to reproduce this condition by varying the voltage knob position and the distance between the electrodes while a video recording of the discharge occurred. The variation of the spark length was evaluated through ImageJ software (1.53 k Version) on different frames obtained from the video recordings. The best setups were used to treat the PP specimens and involved the voltage knob at half of a turn and 4 mm, 9 mm, and 18 mm electrode distances. Additionally, different exposition times were considered, i.e., 5 s, 10 s, 30 s, 60 s, and 120 s. The treatment was carried out under a chemical fume hood at atmospheric laboratory conditions.

The effectiveness of corona treatment is limited in time (aging) due to the reorientation of the polar molecules, which causes a decrease in the surface free energy (increase in hydrophobicity) [10,19]. For this reason, the characterization of the corona-treated PP specimens and the manufacturing of corona-treated PP composites were performed immediately after the treatment.

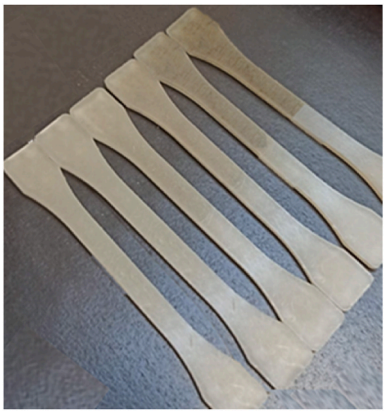

Fig. 4. Macroscopic overview of LASER-treated PP specimens from 5% of laser power (left side) to 40% of laser power (right side).

2. Composite samples for pullout test

A pullout test on the composite samples was carried out to highlight the effectiveness of surface treatments in improving PP-to-matrix adhesion. For this mechanical test, the best corona discharge treatment (18 mm electrode distance and 120 s exposure) and the best UV-LED treatment (36 h) were considered. The pullout test of LASER-treated composite samples is part of an ongoing experimental campaign and is not discussed in this work. Two commercially available premixed mortars were used to manufacture the pullout specimens: a Natural Hydraulic Lime mortar (Geocalce G antisismico by Kerakoll S.p.A) and a cementitious mortar (Geolite by Kerakoll S.p.A). Water-to-premixed mortar ratios of 0.2 and 0.204, respectively, were considered as prescribed by the technical data sheets of the commercial products. The premixed mortars were mixed with water for 1 min at 220 rpm and 4 min at 330 rpm using an axial-flow automatic mixer (RW20 DZM, IKA-Werke GmbH & Co. KG, Staufen, Germany). The so-obtained mortars were poured into silicon cubic molds ($50 \times 50 \times 50$ mm^3) and vibrated on a portable vibrating plate (Controls Group) for 3 min at maximum speed. One end of the dog-bone PP specimens was cut, and the 5 mm-constant mid-section was embedded 30 mm into the fresh mortar cubes. A metal frame consisting of vertical support brackets and horizontal bolted plates was designed and used to maintain the verticality of the PP dog-bone specimens during the composite sample preparation and curing (Fig. 6a). The composite samples were clamped to the horizontal plates for one day while covering with a plastic sheet. Then the composite samples were demolded, removed from the structure, and cured for 7 days in a climatic chamber (20 °C and RH 90%) and lately 21 days at laboratory conditions, covered with a plastic sheet. Fig. 6b shows the demolded samples after the 28-day curing.

The pullout test was performed at 28 days using a UTM Instron 5567 equipped with a 30 kN load cell. The test was carried out at a 2 mm/min displacement rate under displacement control, and the data were collected by Bluehill software. The PP specimen was gripped with an upper pneumatic clamp (Fig. 7a). While the hardened mortar cube was constrained to a purpose-built steel hollow device with an upper hole for the passage of the PP specimen and which was fixed to a lower clamp (Fig. 7b). Four composite samples for each type of mortar and surface treatment were produced and pullout tested. The mechanical results of each composite sample were expressed in terms of load-displacement curve, maximum peak load, residual load (at 25 mm displacement), and deformation energy (until 25 mm displacement). The average value and standard deviation were also evaluated. To further compare the effect of improved adhesion, scanning electron microscopy micrographs (ESEM Quanta 200, Fei Company, Oxford Instruments) detected the number of mortar particles adhering to the treated PP surfaces after pullout in comparison with the untreated ones.

3. Results and discussion

The results obtained from the contact angle measurements are summarized in Fig. 8 for UV-LED (Fig. 8a), picosecond LASER (Fig. 8b) and corona discharge treatment (Fig. 8c). The graphs show the average contact angle results (bar charts) and the associated standard deviations (error bars). As can be seen in Fig. 8a, the effectiveness of UV-LED in improving the PP wettability occurred with increasing exposition time. The best contact angle reduction was around −10% compared to the reference PP specimen (around 105°deg). Although there was an actual reduction in the contact angle, the low improvement value can be related to the glossy surface of the specimens. In fact, the brightness resulting from the surface polishing phase may have partially

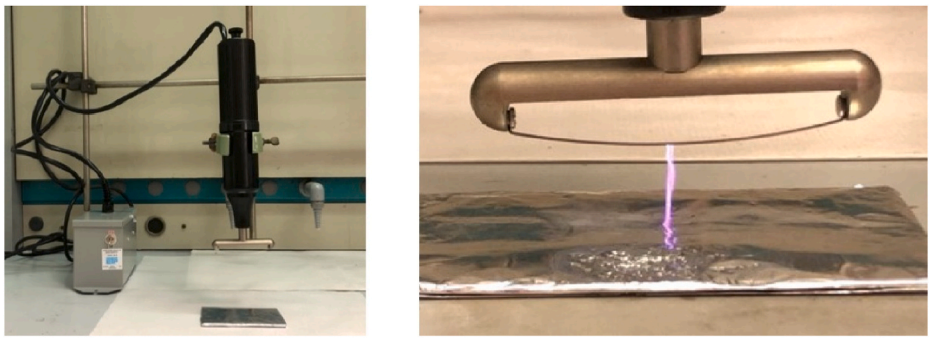

(a) (b)

Fig. 5. Corona discharge treatment: a) treatment setup, b) spark discharge between the electrodes.

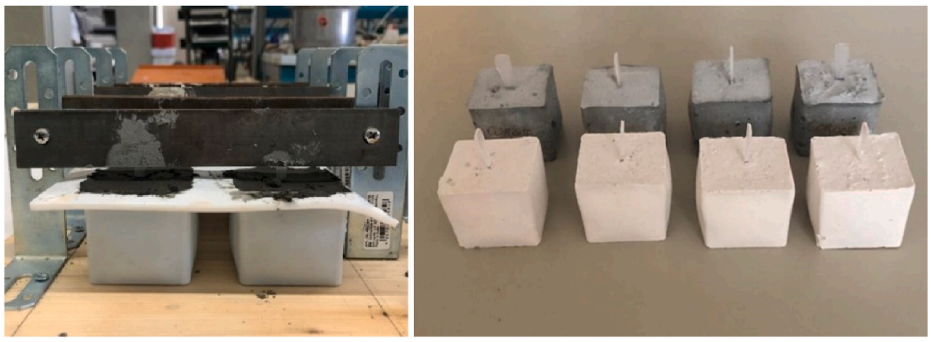

(a) (b)

Fig. 6. Pullout composite samples: a) manufacturing setup for the vertical embedment of PP dog-bone specimens into the cementitious matrix and b) pullout composite samples with Geolite (dark grey) and Geomalta (white).

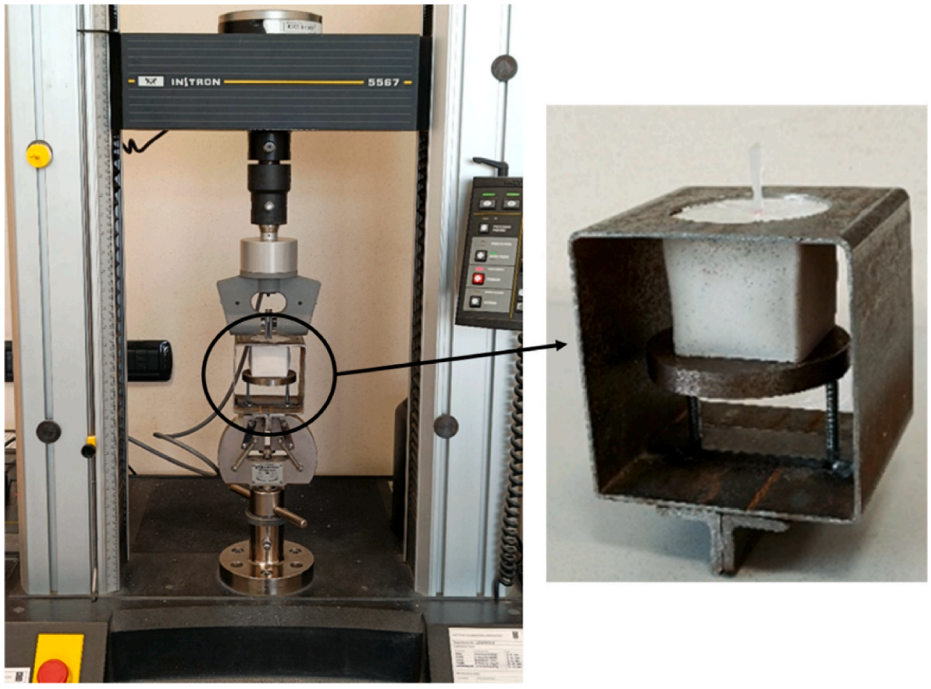

(a) (b)

Fig. 7. Pullout testing setup: a) overall setup using UTM, b) retaining device for the mortar cube.

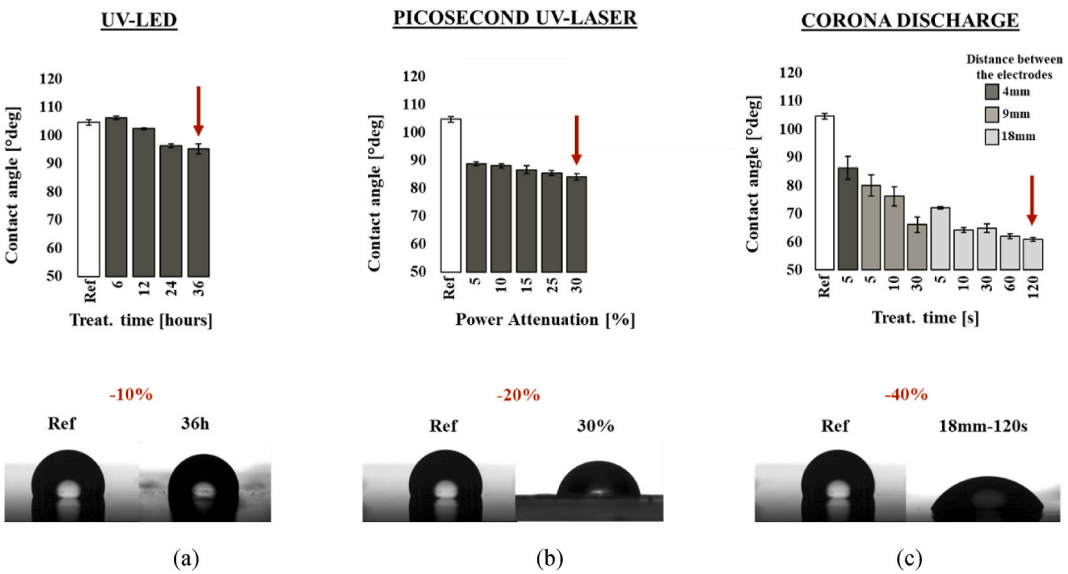

Fig. 8. Contact angle results for PP specimens treated by a) UV-LED, b) picosecond LASER, and c) corona discharge. The error bars stand for standard deviation error.

contributed to the reflection of the UV-LED source and thus mitigated its effect.

Regarding the picosecond LASER treatment, a wettability increase was displayed as the LASER power increased (Fig. 8b). The maximum decrease in contact angle of about 20% was obtained considering a LASER power by 30% (see Table 2). The reduction in contact angle was also observed by Rivero et al. [17] and Buchman et al. [18] for PP surfaces treated with ultrashort LASER.

The corona discharge treatment was more effective in reducing the contact angle of PP as the electrode distance and exposition time increased (Fig. 8c). Notably, a reduction in contact angle of up to 40% (for electrode distance of 18 mm and treatment time of 120 s) was observed. The best treatment conditions (and nomenclature assigned) resulting from the contact angle measurements are shown in Table 3.

The ATR-FTIR also identified the functionalization effect promoted by the PP surface treatments (Fig. 9) by detecting carboxyl (-COOH), carbonyl (C═O), hydroxyl (O–H) and ester (–COO–) groups. [11,12]. Remarkably, the infrared spectroscopy confirmed the same trend in improving the PP surface functionalization as from the contact angle measurement, and the best treatment conditions are the same of Table 3. The main results from the ATR-FTIR characterization of corona-treated specimens are displayed in Fig. 9 and stand as a representative overview also for UV-LED and picosecond LASER results. As the electrode distance and exposition time (and exposition time for UV-LED and LASER power for picosecond LASER treatment) increased, the intensity of the characteristic peaks related to functional groups increased, i.e., carbonyl, hydroxyl, and carboxyl ester. At the same time, those of the polypropylene structure decreased (Fig. 9a). Precisely, a peak increase is observed at 3200–3500 (-OH), 1630–1720 (C═O), 970–1250 (C–O), while a peak decrease at 2850–3000 and 1350–1470 (CH_2, CH_3, CH) and 2700–2840 (C–H) occurred. [11,12]. To better highlight the functionalization effect, Fig. 9b compares the ATR-FTIR spectra of the untreated reference specimen (red line) and the one treated with optimal corona treatment condition (green line).

On the other hand, no morphological surface alterations resulting from the treatments were observed through optical microscopy (Fig. 10). Hence, it was concluded that the involved functionalization was mainly chemical. Fig. 10a shows the surface of untreated PP, while Fig. 10b that of a representative treated PP specimen (optimal corona discharge treatments). All the treatments involved did not cause any significant morphological alteration.

The chemical functionalization of PP enhanced the mechanical performance of PP composites. Indeed, the improved chemical affinity of PP with the surrounding matrix allowed for better adhesion and, thus, the frictional interaction between the phases [6]. As a result, an overall improvement in the load-displacement curve was observed for both lime-based (Fig. 11a) and cement-based composites (Fig. 11b).

The untreated PP composite with lime-based mortar (light grey line, Fig. 11a) was less performing than that with cement-based mortar (light grey line, Fig. 11b). Remarkably, the UV-LED treatment was particularly effective in the lime-based mortar and allowed to reach maximum peak load, residual load and deformation energy comparable to that of cement-based composites (Figs. 12–14). Whereas no significant increase in maximum peak load and residual load was displayed for corona-treated PP composites in lime-based mortar.

On the other hand, the treatments slightly improved the maximum peak load for cement-based composites (Fig. 12b). As a result, treated-PP composites displayed higher resistance than untreated ones to the first tensile cracking.

Most notably, significant improvements in residual load and deformation energy were obtained for treated PP composites compared to untreated ones (Figs. 13 and 14). In detail, UV-LED improved by +134% and +66% the residual load of untreated lime-based (Fig. 13a) and cement-based composites (Fig. 13b), respectively. And corona discharge increased the residual load of cement-based composite by +45% (Fig. 13b). Deformation energy enhancements by +129% and +19% were recorded for UV-LED composites with lime-based mortar (Fig. 14a) and cement-based mortar (Fig. 14b), respectively. On the other hand, the same parameter was raised by corona discharge treatment by +46% and +22% for lime-based mortar (Fig. 14a) and cement-based mortar (Fig. 14b), respectively. Hence, the functionalization treatments promoted toughness and the capability of absorbing higher energy before failure. This is a desirable feature in composite materials like FRC; indeed, it indicates good adhesion and stress transfer from the brittle matrix to the more ductile reinforcement.

Table 3
Best treatment conditions for UV-LED, picosecond LASER, and corona discharge treatments obtained from the contact angle measurements.

Treatment	Best conditions	Specimen Nomenclature
UV-LED	36 h – exposition time	UV-LED 36
Picosecond LASER	30% - LASER power	LASER 30
Corona discharge	18 mm - electrode distance 120 s - exposition time	CORONA 18-120

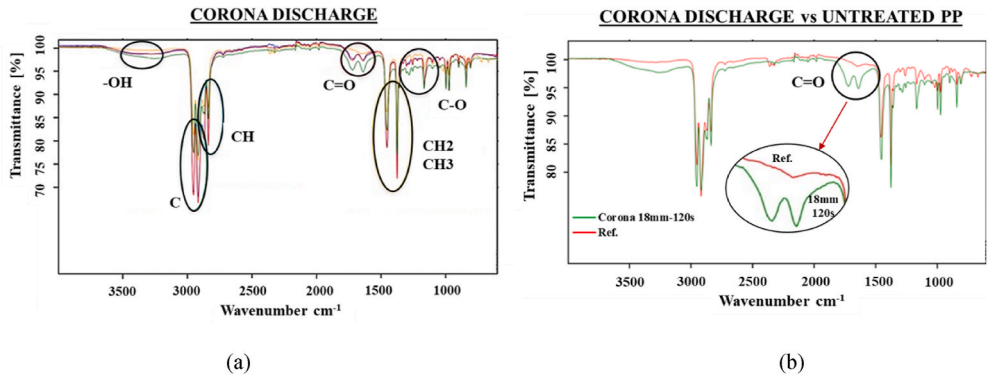

Fig. 9. ATR-FTIR spectra results of a) all corona discharge-treated PP specimens and b) the best corona discharge treatment compared to the reference untreated PP specimen.

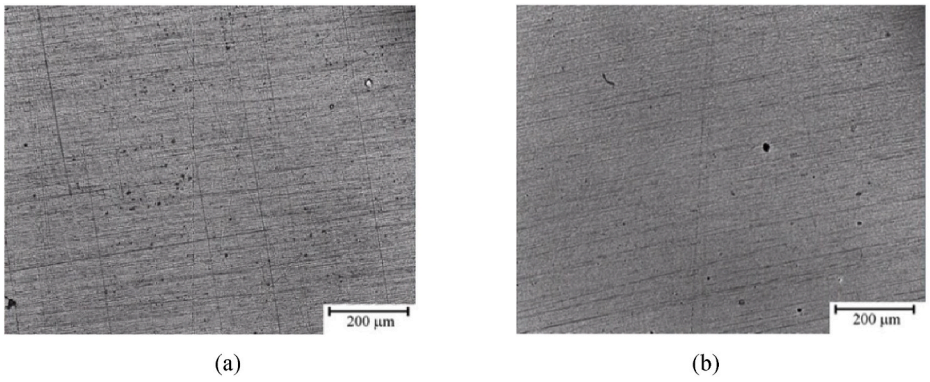

Fig. 10. Optical micrographs at 100x magnitude registering no surface morphological alteration a) before and b) after the surface treatments. In Fig. 10b, the corona discharge-treated surface is reported as representing all other surface treatments.

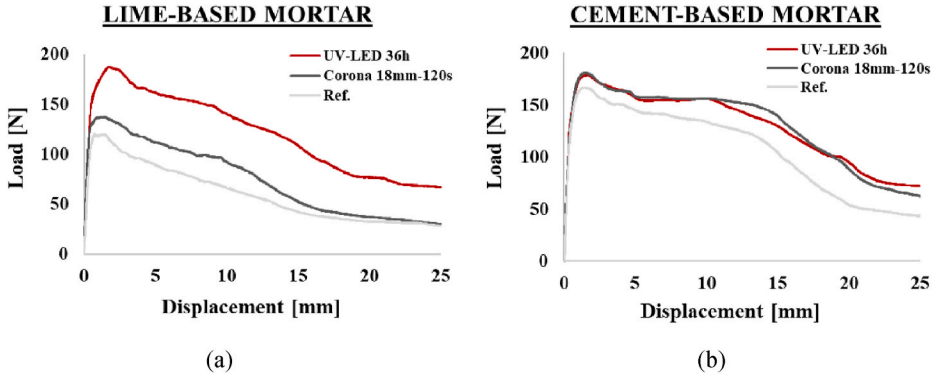

Fig. 11. Load-displacement curves resulting from the pullout test of PP composite samples manufactured with a) lime-based mortar and b) cement-based mortar.

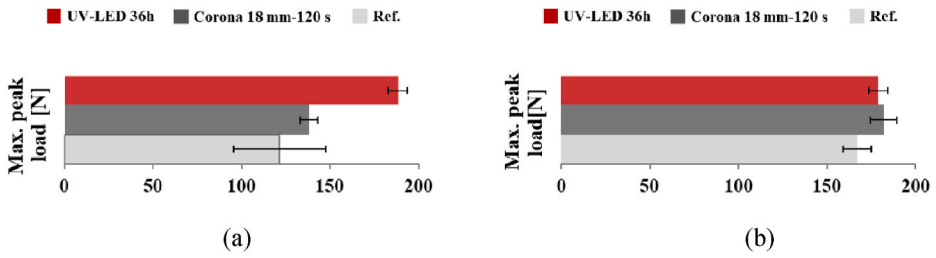

Fig. 12. Maximum peak load resulting from the pullout test of PP composite samples manufactured with a) lime-based mortar and b) cement-based mortar. The error bars stand for standard deviation error.

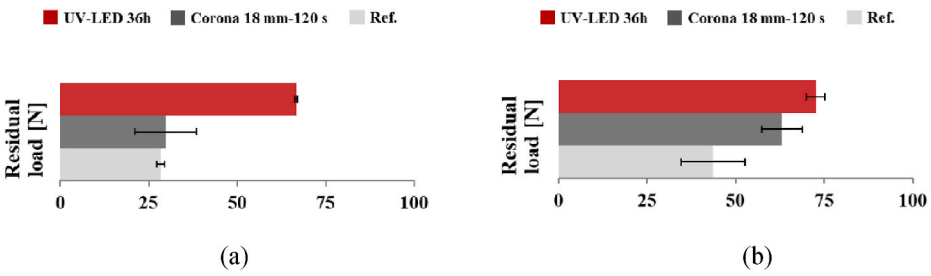

Fig. 13. Residual load (at 25 mm displacement) resulting from the pullout test of PP composite samples manufactured with a) lime-based mortar and b) cement-based mortar. The error bars stand for standard deviation error.

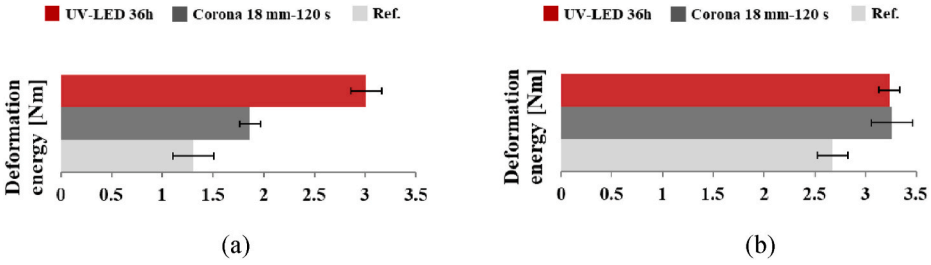

Fig. 14. Deformation energy (until 25 mm displacement) resulting from the pullout test of PP composite samples manufactured with a) lime-based mortar and b) cement-based mortar. The error bars stand for standard deviation error.

The functionalized surfaces provided a chemical adhesion with the surrounding matrix, the effectiveness of which was evaluated by observing the number of mortar particles to the PP specimen after pullout from the matrix. Confirming the mechanical results and chemical functionalization evidence, the treated PP specimens (Fig. 15b) showed more mortar particles adhering to the surface after the pullout test than the untreated ones (Fig. 15a). So, the failure of the treated PP composites occurred at higher deformation energy and within the interfacial transition zone (ITZ) allowing for a better stress distribution between the bulk matrix and the reinforcement. This means that the treatments promoted stronger adhesion between the phases and a higher shear frictional strength during pullout [20]. Conversely, the failure occurred through debonding and slipping from the matrix for the untreated PP composites (no mortar particles adhering, Fig. 15a) [21]. Confirming the literature findings, the modified adhesion between the PP reinforcement and matrix influenced the deformation mechanism of the reinforcement and, consequently, the failure mode of the composite [5].

4. Conclusions

Several chemical surface treatments have been studied to improve the poor adhesion of PP with cementitious matrix, thus promoting PP fibers as an alternative to steel fibers in fiber-reinforced concrete (FRC). For the first time, this work suggested more sustainable (no chemicals added), fast, cost-efficient, and industrially scalable surface treatments (UV-LED, picosecond UV-LASER, and corona discharge) aimed at improving the adhesion between PP and cementitious matrix. Increasing exposition time from 6 h to 36 h, LASER power from 0% to 30%, and electrode distance from 4 mm to 18 mm with exposition time from 5 s to 120 s were considered for UV-LED, picosecond UV-LASER, and corona discharge, respectively. The most effective setups and exposition parameters were identified, and the main characterization results showed that:

- For ATR-FTIR spectroscopy, all treatments increased the PP hydrophilicity by altering the surface chemical structure (oxidation and photooxidation) and providing C═O, C═O, –OH bonds.

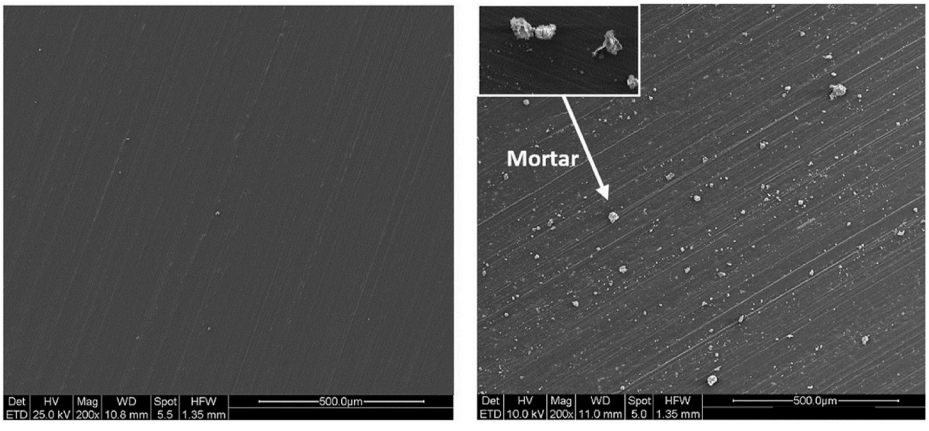

Fig. 15. ESEM images at 200x showing the number of mortar particles adhering on the PP surface after the pullout test for a) untreated PP and b) treated PP.

Additionally, all treatment conditions reduced the contact angle compared to the untreated PP surface.

- The highest oxides FTIR peaks intensity and contact angle reduction set the optimized treatment conditions, namely 36 h for the UV-LED, 30% LASER power for the picosecond UV-LASER, and 18 mm electrode distance and 120 s for the corona discharge. Notably, the contact angle of PP was reduced by 10% up to 40%.
- The involved treatments resulted in the functionalization of the surface without altering its morphology. So, a chemical rather than a physical adhesion with the cementitious matrix was expected.
- The optimized treatment conditions of UV-LED and corona discharge treatments enhanced the pullout performance of PP composite samples. The residual load and deformation energy were significantly increased, and numerous mortar particles remained adhering to the treated PP surface as proof of better adhesion. Because of a better phase interaction, the failure mode changed from slipping from the matrix (untreated PP) to cracking in the interphase zone (treated PP). UV-LED and corona discharge treatments were equally effective in cement-based composites, while UV-LED was more effective than corona discharge in lime-based composites.

These promising results highlighted the feasibility of optimizing the mechanical performance of PP-FRCs by enhancing the chemical adhesion between PP and cementitious matrixes. Significant improvements, such as the change in failure mode, were observed for all the surface treatments involved. Remarkably, the possibility of considering non-chemical reactants and easy, fast, and cost-efficient setup conditions was pointed out for the first time to increase PP wettability and hydrophilicity. The present analysis is being further investigated for LASER treatment in an ongoing experimental campaign, evaluating the effects induced by surface topographical alteration at micro and nanoscales (i.e., grooves, grids, and holes) in addition to chemical functionalization.

Declaration of competing interest

The authors declare that they have no known competing financial interests or personal relationships that could have appeared to influence the work reported in this paper.

Acknowledgements

The authors would like to thank Professor Leonardo Orazi and Professor Barbara Reggiani, who provided insight and expertise on LASER treatments that greatly assisted the research. Acknowledgements are also extended to Kerakoll S.p.A. for supplying the mortars used for the pullout test.

References

[1] A. Favier, C. De Wolf, et al., A sustainable future for the European Cement and Concrete Industry. Technology assessment for full decarbonisation of the industry by 2050, ETH Zurich (2018), https://doi.org/10.3929/ethz-b-000301843.
[2] B. Ralph, H.C. Yuen, W.B. Lee, The processing of metal matrix composites - an overview, J. Mater. Process. Technol. 63 (1997) 339–353, https://doi.org/10.1016/S0924-0136(96)02645-3.
[3] S. Maitra, Nanoceramic matrix composites: types, processing and applications, in: I.M. Low (Ed.), Advances in Ceramic Matrix Composites, Woodhead Publishing, 2014, pp. 691–709.
[4] J. Cho, A.R. Boccaccini, M.S.P. Shaffer, Ceramic matrix composites containing carbon nanotubes, J. Mater. Sci. 44 (2009) 1934–1951, https://doi.org/10.1007/s10853-009-3262-9.
[5] V. Zacharda, J. Němeček, P. Štemberk, Micromechanical performance of interfacial transition zone in fiber-reinforced cement matrix, IOP Conf. Ser. Mater. Sci. Eng. 246 (2017), 012018, https://doi.org/10.1088/1757-899X/246/1/012018.
[6] Z. Lin, V.C. Li, Crack bridging in fiber reinforced cementitious composites with slip-hardening interfaces, J. Mech. Phys. Solid. 45 (5) (1997) 763–787, https://doi.org/10.1016/S0022-5096(96)00095-6.
[7] Z. Zheng, D. Feldman, Synthetic fibre-reinforced concrete, Prog. Polym. Sci. 20 (2) (1995) 185–210, https://doi.org/10.1016/0079-6700(94)00030-6.
[8] C. Signorini, A. Sola, B. Malchiodi, A. Nobili, Highly dissipative fiber-reinforced concrete for structural screeds, J. Mater. Civ. Eng. 34 (4) (2022), 04022022, https://doi.org/10.1061/(ASCE)MT.1943-5533.0004160.
[9] L. Akand, M. Yang, X. Wang, Effectiveness of chemical treatment on polypropylene fibers as reinforcement in pervious concrete, Construct. Build. Mater. 163 (2018) 32–39, https://doi.org/10.1016/j.conbuildmat.2017.12.068.
[10] J. Izdebska, Corona treatment, in: J. Izdebska, S. Thomas (Eds.), Printing on Polymers: Fundamentals and Applications, William Andrew Publishing, 2016, pp. 123–142.
[11] V.C. Louzi, J.S. de C. Campos, Corona treatment applied to synthetic polymeric monofilaments (PP, PET, and PA-6), Surface. Interfac. 14 (2019) 98–107, https://doi.org/10.1016/j.surfin.2018.12.005.
[12] N. Sellin, J.S. de C. Campos, Surface composition analysis of PP films treated by corona discharge, Mater. Res. 6 (2) (2003) 163–166, https://doi.org/10.1590/s1516-14392003000200009.
[13] L. Orazi, L. Romoli, M. Schmidt, L. Li, Ultrafast laser manufacturing: from physics to industrial applications, CIRP Ann 70 (2) (2021) 543–566, https://doi.org/10.1016/j.cirp.2021.05.007.
[14] A. Riveiro, P. Pou, et al., Laser texturing to control the wettability of materials, Procedia CIRP 94 (2020) 879–884, https://doi.org/10.1016/j.procir.2020.09.065.
[15] A.O. Ijaola, E.A. Bamidele, et al., Wettability transition for laser textured surfaces: a comprehensive review, Surface. Interfac. 21 (2020), 100802, https://doi.org/10.1016/j.surfin.2020.100802.
[16] A. Riveiro, A.L.B. Maçon, J. del Val, et al., Laser surface texturing of polymers for biomedical applications, Front. Physiol. 6 (2018) 16, https://doi.org/10.3389/fphy.2018.00016.
[17] A. Riveiro, R. Soto, et al., Texturing of polypropylene (PP) with nanosecond lasers, Appl. Surf. Sci. 374 (2016) 379–386, https://doi.org/10.1016/j.apsusc.2016.01.206.
[18] A. Buchman, M. Rotel, H. Dodiuk, Nd: YAG laser surface treatment of various materials to enhance adhesion, in: K.L. Mittal, T. Bahners (Eds.), Laser Surface Modification and Adhesion, Scrivener Publishing LLC, 2014, pp. 1–53.
[19] J.E. Klemberg-Sapieha, L. Martinu, S. Sapieha, M.R. Wertheimer, Control and modification of surfaces and interfaces by corona and low pressure plasma, in: G. Akovali (Ed.), The Interfacial Interactions in Polymeric Composites, Springer, Dordrecht, 1993, pp. 201–222.
[20] P. Di Maida, C. Sciancalepore, E. Radi, F. Bondioli, Effects of nano-silica treatment on the flexural post cracking behaviour of polypropylene macro-synthetic fibre reinforced concrete, Mech. Res. Commun. 88 (2018) 12–18, https://doi.org/10.1016/j.mechrescom.2018.01.004.
[21] C. Signorini, A. Sola, B. Malchiodi, A. Nobili, A. Gatto, Failure mechanism of silica coated polypropylene fibres for Fibre Reinforced Concrete (FRC), Construct. Build. Mater. 236 (2020), 117549, https://doi.org/10.1016/j.conbuildmat.2019.117549.